Search for the production of dark matter in the framework of a mono-Z′ portal at the ILC with simulated electron-positron collisions at $\sqrt{s} = 500$ GeV

S. Elgammal*

Centre for Theoretical Physics, The British University in Egypt, P.O. Box 43, El Sherouk City, Cairo 11837, Egypt

(Received 24 April 2024; accepted 1 August 2024; published 11 September 2024)

In the present work, we study the possible production of the light neutral gauge boson (Z′) candidates, which originated from a simplified-model scenario based on the mono-Z′ model, in association with dark matter. This study has been performed by studying events with dimuon plus missing transverse energy produced in the simulated electron-positron collisions at the foreseen International Linear Collider (ILC), operating at 500 GeV center of mass energy and integrated luminosity of 1000 fb^{-1}. In case no new physics has been discovered, we set upper limits at 95% confidence level on the masses of various particles in the model as, spin-1 (Z′), as well as the fermionic dark matter.

DOI: 10.1103/PhysRevD.110.055020

I. INTRODUCTION

The Standard Model of particle physics (SM) has succeeded in describing many features of nature that we observe in our experiments [1]. The most famous example, arguably, is the agreement between the SM prediction and the experimental measurement of the electroweak theory, which led to the old discovery of $W^{\pm}$, Z^0 bosons and the recent discovery of the SM Higgs boson by ATLAS experiment [2] and CMS experiment [3].

Although its success, SM is well known that it is not a complete theory. It describes only the visible, baryonic, matter in the Universe, which represents about 5% of the energy density distribution content of the Universe. The rest is attributed to the mysterious dark energy and dark matter (DM). Many cosmological observations, based on recent observations by [4–6], support the existence of dark matter. These observations suggest that dark matter is non-decaying and weakly interacting massive particles. So, SM could be considered as a low-energy manifestation of other theories realized at high energy, generically known as BSM (beyond the Standard Model) theories [7].

Both the ATLAS and CMS collaborations have previously searched for the massive extra neutral gauge boson Z′, which is induced by the grand unified theory (GUT) and supersymmetry [8–11], with no evidence of their existence using the full RUN II period of the LHC data [12,13]. Results by the CMS have excluded, at 95% confidence level (CL), the existence of Z′ in the mass range between 0.6–5.15 TeV, while the ATLAS experiment has excluded the mass range between 0.6–5.1 TeV.

In addition, many searches for DM have been performed by analyzing the data collected by the CMS and ATLAS experiments during RUN II. These searches rely on the production of a visible object "X", which recoils against the large missing transverse energy from the dark matter particles leaving a signature of $(X + E_T^{\text{miss}})$ in the detector [14]. The visible particle could be an SM particle like W, Z bosons or jets [15,16], photon [17,18] or SM Higgs boson [19–21].

The current collider experiments, including ATLAS and CMS, have set strict limitations on the coupling of the Z′ particle to the standard model (SM) leptons (g_l). Based on the observation of 4-muon final states [22,23], the coupling constant g_l is ruled out in the range of 0.004 to 0.3, depending on the mass of the Z′ boson. Furthermore, at high Z′ mass ($M_{Z'} > 200$ GeV), the ATLAS collaboration searched for dark matter within the framework of the mono-Z′ model [24], specifically in the leptonic decay channel of Z′ at the LHC [25]. This search has excluded Z′ masses between 200 and 1000 GeV and placed distinct constraints on g_l. Hence, within the light-vector scenario, g_l is excluded in the range of 0.01–0.025 for lower Z′ masses and 0.02–0.38 for higher Z′ masses between 200 to 1000 GeV. Data from previous colliders, such as the LEP-2 experiment [26], have provided further insights. For Z′ masses greater than the center-of-mass energy ($\sqrt{s} = 209$ GeV), the LEP collaboration has imposed a limit of $g_l \leq 0.044 M_{Z'}/(200\,\text{GeV})$, and for $M_{Z'} < 209$ GeV, $g_l \leq 0.044$ [27].

*Contact author: sherif.elgammal@bue.edu.eg

The constraints on the value of g_l based on dark matter detections from astrophysical and cosmological observations:

(i) For neutrino trident production, the limit is $g_l \leq 1.9 \times 10^{-3} M_{Z'}/\text{GeV}$ [28].
(ii) The LSND experiment obtained a 95% confidence level bound of $g_l \leq 3 \times 10^{-3} M_{Z'}/\text{GeV}$ for neutrino scattering measurements, while the TEXONO experiment set a limit of $g_l \leq 1.7 \times 10^{-3} M_{Z'}/\text{GeV}$ [29,30].
(iii) IceCube's study of Z′ couplings with SM neutrinos and electrons resulted in a nonstandard neutrino interactions (NSI) constraint translating into a bound of $g_l \leq 5.9 \times 10^{-4} M_{Z'}/\text{GeV}$ [31].
(iv) The most recent results from the advanced LIGO-VIRGO run 3, regarding the search for stochastic gravitational waves, have partially excluded the high mass range $M_{Z'} \in [20\ \text{TeV}, 1\ \text{PeV}]$, with a gauge coupling between $g_l \in [0.37, 0.44]$ [27].

However, various constraints on the direct detection of dark matter in underground experiments such as XENON10, XENON100, and XENON1T [32–34], alongside recent findings from SENSEI [35] and PandaX-II [36] regarding light dark matter scattering are presented. As a result, the model suggests that the interaction between dark matter and electrons can be utilized to explore light-dark matter ($M_{\text{DM}} < 1$ GeV). Exclusion limits at a 90% confidence level from these experiments eliminate the possibility of dark matter with masses exceeding 4 MeV [37].

Besides the aforementioned, indirect detection searches for dark matter are currently more exciting than ever. This means that the annihilation of dark matter into leptons or hadrons in space can potentially produce a signal of thermal WIMPs. We outline the most reliable constraints for GeV dark matter annihilation into various final states as follows: Fermi observations of dwarf spheroidal galaxies provide the most stringent constraint on annihilation to hadronic final states [38,39]; AMS-02 positron fluxes limit most annihilation to leptons [40,41], these limits have shown that these analyses are sensitive to the thermal relic cross section for DM particles with mass < 200 GeV; and the CMB [42] limits are most pronounced for low dark matter masses (below about 10 GeV) [43,44]. Based on these results, the WIMP DM mass window from 20 GeV up to the unitarity limit [45] of 100 TeV remains largely open [46,47].

If the Z′ does not couple to quarks, the HL-LHC and future hadron colliders would provide no limits on the existence of Z′. Then the future electron-positron colliders as the foreseen International Linear Collider (ILC) will play an important role.

The ILC is an electron-positron collider, which has been proposed to operate at 500 GeV center of mass energy ($\sqrt{s}$) as a startup with possible upgrade to $\sqrt{s} = 1000$ GeV in run II [48–51]. The linear electron-positron colliders are characterized by controllable initial particle energy, low QCD background compared to hadron colliders, and controllable beam polarization.

In this analysis, we present a search for light neutral gauge bosons (Z′) (i.e., $M_{Z'} < 90$ GeV), which are originated from a simplified-model scenario, which is known as the light vector (LV), in the framework of mono-Z′ model [24], at the ILC simulated electron-positron collisions with 500 GeV center of mass energy. The topology of the studied simulated events is dimuon, from the decay of Z′, plus large missing transverse energy attributed to dark matter. A similar analysis has been presented for searching for dark matter in association with the visible particle being a Z boson decaying to dimuon at the ILC [52].

In this paper, we will first present the theoretical framework of the simplified model based on the mono-Z′ portal and its free parameters in Sec. II. Next, we will explain the simulation techniques used for generating events for both the signal and the SM background samples in Sec. III. We will then discuss the selection cuts and the analysis strategy in Sec. IV. Finally, we will present the results and provide a summary of this analysis in Secs. V and VI, respectively.

II. THE SIMPLIFIED MODEL IN THE FRAMEWORK OF MONO-Z′ PORTAL

The mono-Z′ model, discussed in [24], assumes that dark matter is produced from electron-positron collisions at the ILC via a new light gauge boson Z′. In the mono-Z′ model, the dark matter can be produced through three different scenarios.

This model considers two scenarios with a minimal set of renormalizable interactions. The first scenario involves dark-Higgsstrahlung from a Z′, where the dark Higgs decays invisibly. The second scenario involves a dark sector with two states, $\chi_{1,2}$, which couple off-diagonally to the Z′. In terms of renormalizable scenarios, the $Z' + E_T^{\text{miss}}$ search demonstrates better sensitivity than direct resonance searches, particularly for low Z′ masses [24]. This analysis will exclusively focus on the second light vector (LV) scenario, as illustrated in Fig. 1.

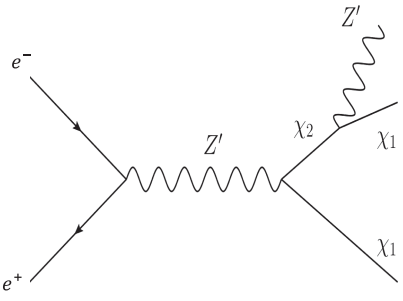

FIG. 1. Feynman diagram for the Light Vector (LV) scenario based on mono-Z′ model; for the production of neutral light gauge boson (Z′) in association to dark matter (χ_1) pair [24].

The proposed dark matter can be produced through the process of pair annihilation of electron-positron mediated by a light vector boson Z′, which then undergoes two dark matters, a light dark matter (χ_1) and a heavy one (χ_2). χ_2 is heavy enough to decay to a Z′ and another light dark matter χ_1 (i.e., $\chi_2 \to Z'\,\chi_1$) as shown in Fig. 1.

The interaction term, in the Lagrangian, between the dark fermions and Z′ is given by [24]

$$\frac{g_{DM}}{2} Z'_\mu(\overline{\chi_2}\gamma^\mu\gamma^5\chi_1 + \overline{\chi_1}\gamma^\mu\gamma^5\chi_2),$$

where g_{DM} is the coupling of Z′ to the dark matter χ_1 and χ_2. In the rest of the paper, the notation (χ) refers to (χ_1). For future reference, the coupling of the Z′ to the visible leptons will be represented by g_l, while the coupling of the Z′ to the dark matter will be represented by g_{DM} in the rest of this paper.

The only allowed decays in the LV scenario are assumed to be the decay of $Z' \to \chi_1\chi_2$, $\chi_2 \to Z'\chi_1$ and $Z' \to \mu^+\mu^-$. Where the total decay width of the Z' and χ_2 can be calculated given the values of the masses of Z' and dark matter and the coupling constants.

The free parameters in this scenario are the lightest dark matter mass M_{χ_1}, M_{χ_2}, the Z′ mass ($M_{Z'}$) and the coupling of Z′ to both leptons and dark matter particles g_l and g_{DM} respectively.

The CMS and ATLAS detectors have conducted intensive searches for Z′ over many years. As a result, it has been proven that heavy neutral gauge bosons (Z′) do not exist in the mass range between 0.2 to 5.15 TeV. Therefore, we focus our investigation on the production of light neutral gauge bosons (Z′) in the mass range below 90 GeV at the ILC.

To achieve this, the LV scenario has been considered with the use of the light-dark sector case for acquiring mass to dark matter particles (χ_1 and χ_2) as presented in Table I. This is a specific choice made to fix M_{χ_1} and M_{χ_2} according to a prescription given in [24]. It is important to note that this is only one of the possible choices.

Due to previous restrictions on the value of g_l from different experiments as the CMS, ATLAS, and LEP-2 in the range of $M_{Z'}$ values between 10 and 80 GeV, g_l needs to be approximately 0.003 [27]. According to [24], g_{DM} is equal to 1.0. While the values of the masses ($M_{Z'}$, M_{χ_1}, and M_{χ_2}) are not fixed but are scanned over.

Two leptons identify the signal of the processes being studied with opposite charges. These leptons are created from the decay of Z′ and are accompanied by a large amount of missing transverse energy caused by the stable dark matter χ_1. Therefore, the events we are examining can be described as having the topology of ($\mu^+\mu^- + E_T^{\text{miss}}$).

TABLE I. The light mass assumptions for the dark sector for the light vector scenario [24].

Scenario	Masses assumptions
Light dark sector	$M_{\chi_1} = 1, 5, \ldots, 200$ GeV $M_{\chi_2} = M_{\chi_1} + M_{Z'} + 25$ GeV

III. SIMULATION OF SIGNAL SAMPLES AND SM BACKGROUNDS

The SM background processes yielding muon pairs in the signal region are Drell-Yan (DY $\to \mu^+\mu^-$) production, the production of top quark pairs ($t\bar{t} \to \mu^+\mu^- + 2b + 2\nu$) and production of diboson ($W^+W^- \to \mu^+\mu^- + 2\nu$, $ZZ \to \mu^+\mu^- + 2\nu$ and $ZZ \to 4\mu$).

The LV scenario signal samples and corresponding SM background processes were generated using WHIZARD event generator 3.1.1 [53]. The ISR effect was included and interfaced with Pythia 6.24 for parton shower model and hadronization [54]. For a fast detector simulation of ILD detector, DELPHES package [55] was used. These were generated from electron-positron collisions at the ILC with a 500 GeV center of mass energy, which corresponds to the circumstances of RUN I. The polarized degrees of electron and positron beams are $P_{e^-} = 0.8$ and $P_{e^+} = -0.3$, respectively.

For the scenario where light vectors are produced along with dark matter particles (χ_1 and χ_2), we have considered the mass assumptions as summarized in Table I. Assuming $g_l = 0.003$ and $g_{DM} = 1.0$, Table II shows the production cross section times branching ratios at leading order (LO) for various mass points of Z′ and DM. The polarized degrees of electron and positron beams are $P_{e^-} = 0.8$ and $P_{e^+} = -0.3$, respectively, at the ILC with $\sqrt{s} = 500$ GeV.

In Fig. 2, the production cross sections multiplied by branching ratios are plotted against the mass of the dark matter (M_{χ_1}) for two different Z′ mass points ($M_{Z'} = 20$ and 80 GeV). These signal samples were generated at the ILC with $\sqrt{s} = 500$ GeV, and the electron-positron beams polarization was $P_{e^-} = 0.8$ and $P_{e^+} = -0.3$, respectively. This graph shows that the cross sections multiplied by branching ratios remain relatively flat until the mass of the dark matter reaches 100 GeV. After that point, they decrease rapidly.

Figure 3 illustrates the cross sections times branching ratios against the mass of the neutral gauge boson (Z′) for three different dark matter mass values: 1 GeV, 100 GeV, and 200 GeV. It has been observed that there is a significant decrease in the cross sections times branching ratios as the dark matter mass increases, while the mass of Z′ also affects this trend.

The Monte Carlo simulations were used to generate the SM background samples and calculate their corresponding cross sections for this analysis. The calculations were done in leading order and can be found in Table III. The signal samples and SM background processes were estimated from these simulations and were normalized to their

TABLE II. The light vector scenario production cross sections times branching ratios (in fb) at leading order (LO) for different choices of the DM mass M_{χ_1} (in GeV) and Z′ mass $M_{Z'}$ (in GeV); for the light-dark sector mass assumption with the following couplings constants $g_l = 0.003$, $g_{DM} = 1.0$. Given that the polarized degrees of electron and positron beams are $P_{e^-} = 0.8$, $P_{e^+} = -0.3$ at the ILC with $\sqrt{s} = 500$ GeV.

	$M_{Z'}$								
M_{χ_1}	10	20	30	40	50	60	70	80	90
1	7.73×10^{-1}	7.08×10^{-1}	6.73×10^{-1}	6.49×10^{-1}	6.28×10^{-1}	6.12×10^{-1}	6.01×10^{-1}	5.88×10^{-1}	5.78×10^{-1}
5	7.63×10^{-1}	6.87×10^{-1}	6.52×10^{-1}	6.29×10^{-1}	6.09×10^{-1}	5.95×10^{-1}	5.82×10^{-1}	5.70×10^{-1}	5.60×10^{-1}
10	7.62×10^{-1}	6.65×10^{-1}	6.30×10^{-1}	6.05×10^{-1}	5.86×10^{-1}	5.73×10^{-1}	5.59×10^{-1}	5.48×10^{-1}	5.39×10^{-1}
25	6.44×10^{-1}	6.20×10^{-1}	5.75×10^{-1}	5.47×10^{-1}	5.27×10^{-1}	5.12×10^{-1}	4.98×10^{-1}	4.86×10^{-1}	4.76×10^{-1}
50	6.35×10^{-1}	5.57×10^{-1}	4.92×10^{-1}	4.59×10^{-1}	4.37×10^{-1}	4.19×10^{-1}	4.03×10^{-1}	3.90×10^{-1}	3.77×10^{-1}
100	6.30×10^{-1}	3.80×10^{-1}	3.15×10^{-1}	2.82×10^{-1}	2.59×10^{-1}	2.40×10^{-1}	2.24×10^{-1}	2.10×10^{-1}	1.94×10^{-1}
125	4.46×10^{-1}	2.69×10^{-1}	2.20×10^{-1}	1.93×10^{-1}	1.73×10^{-1}	1.56×10^{-1}	1.41×10^{-1}	1.28×10^{-1}	1.17×10^{-1}
150	1.85×10^{-1}	1.62×10^{-1}	1.31×10^{-1}	1.11×10^{-1}	9.57×10^{-2}	8.26×10^{-2}	7.07×10^{-2}	5.97×10^{-2}	4.95×10^{-2}
170	1.35×10^{-1}	8.95×10^{-2}	7.07×10^{-2}	5.77×10^{-2}	4.67×10^{-2}	3.72×10^{-2}	2.86×10^{-2}	2.12×10^{-2}	1.48×10^{-2}
175	1.10×10^{-1}	7.41×10^{-2}	5.81×10^{-2}	4.64×10^{-2}	3.68×10^{-2}	2.82×10^{-2}	2.08×10^{-2}	1.45×10^{-2}	9.22×10^{-3}
200	2.48×10^{-2}	1.84×10^{-2}	1.28×10^{-2}	8.08×10^{-3}	4.50×10^{-3}	2.02×10^{-3}	6.27×10^{-4}	1.15×10^{-4}	8.19×10^{-6}

respective cross sections and an integrated luminosity of 1000 fb^{-1}.

An *ad hoc* flat 10% uncertainty is applied to cover all possible systematic effects.

IV. EVENT SELECTION

The event selection process has been designed to reconstruct a final state consisting of two muons with low transverse momentum (p_T) and missing transverse energy accounting for the dark matter candidate. The selection is made by applying cuts on various kinematic parameters.

Both muons must pass a preliminary selection that includes the following criteria:

(i) $p_T^{\mu}(\mathrm{GeV}) > 10$,
(ii) $|\eta^{\mu}|(\mathrm{rad}) < 2.5$,
(iii) IsolationVar < 0.1.

Here, "IsolationVar" represents the isolation cut in DELPHES software to reject muons produced inside jets. This cut requires that the scalar p_T sum of all muon tracks within a cone of $\Delta R = 0.5$ around the muon candidate, excluding the muon candidate itself, should not exceed 10% of the p_T of the muon.

Therefore, each event is selected with two opposite charge muons.

Figure 4 shows the distribution of the dimuon invariant mass; the cyan histogram represents the Drell-Yan background, the yellow histogram stands for the vector boson

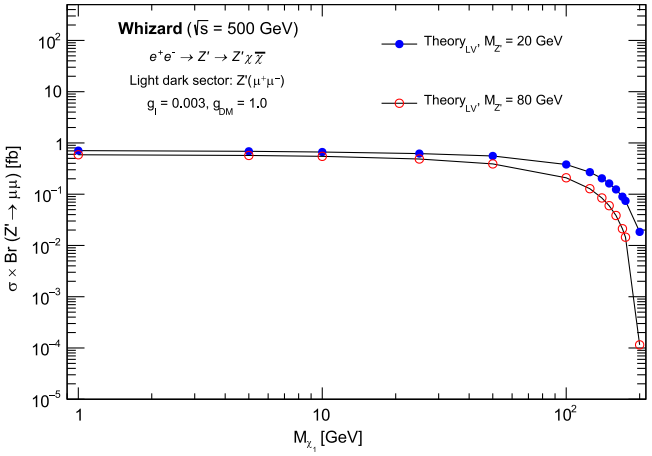

FIG. 2. Dependence of cross sections for the signal process $e^+e^- \to \chi\bar{\chi}Z'(Z' \to \mu^+\mu^-)$ induced by the light vector (LV) on the DM mass with $\sqrt{s} = 500$ GeV and the electron-positron beams polarization are $P_{e^-} = 0.8$, $P_{e^+} = -0.3$. The blue dots refers to $M_{Z'} = 20$ GeV, while the red dots for $M_{Z'} = 80$ GeV.

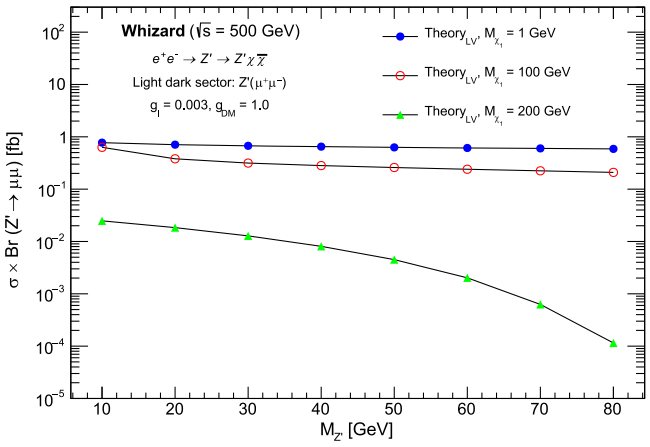

FIG. 3. Dependence of cross sections for the signal process $e^+e^- \to \chi\bar{\chi}Z'(Z' \to \mu^+\mu^-))$ induced by the light vector (LV) on the Z′ mass with $\sqrt{s} = 500$ GeV and the electron-positron beams polarization are $P_{e^-} = 0.8$, $P_{e^+} = -0.3$. The blue dots refers to $M_{\chi_1} = 1$ GeV, the red dots for $M_{\chi_1} = 100$ GeV and the green dots for $M_{\chi_1} = 200$ GeV.

TABLE III. The simulated SM backgrounds generated from electron-positron collisions at the ILC with the polarized degrees of electron and positron beams are $P_{e^-} = 0.8$, $P_{e^+} = -0.3$ at $\sqrt{s} = 500$ GeV. Their corresponding cross section times branching ratio for each process and the generation order are presented. Names of these MC samples and the used generators are stated as well.

Process	Deacy channel	Generator	$\sigma \times$ BR (fb)	Order
DY	$\mu^+\mu^-$	Whizard	1767	LO
$t\bar{t}$	$\mu^+\mu^- + 2b + 2\nu$	Whizard	10.4	LO
WW	$\mu^+\mu^- + 2\nu$	Whizard	232.8	LO
ZZ	$\mu^+\mu^- + 2\nu$	Whizard	3.7	LO
ZZ	4μ	Whizard	0.5	LO

pair backgrounds (WW and ZZ), and the red histogram represents the $t\bar{t}$ background. These histograms are stacked. While the signals of the LV scenario, which have been generated with different masses of the Z′ boson and fixing the dark matter mass ($M_{\chi_1} = 1$ GeV), are represented by different colored lines, and are overlaid.

Figure 5 presents the corresponding distributions of the missing transverse energy for a signal sample with $M_{Z'} = 20$ GeV and $M_{\chi_1} = 1$ GeV, as well as for SM backgrounds. The figure indicates that the signal sample is heavily contaminated with backgrounds across the entire missing transverse energy range. Therefore, it is crucial to implement more stringent criteria to distinguish the signals from SM backgrounds, as explained in the following paragraph.

In addition to the preliminary selection, extra tighter cuts have been applied. These tight cuts are based on four variables: the first variable is related to the invariant mass of the dimuon, at which we restricted the invariant mass of the

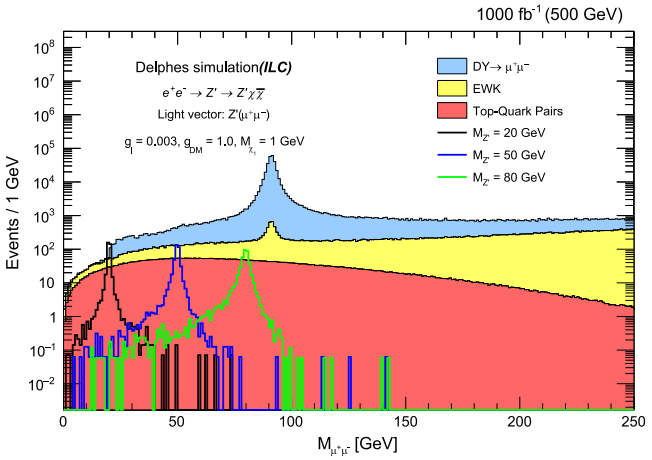

FIG. 4. The measured dimuon invariant mass spectrum, after applying preliminary selection(i) summarized in Table IV, for the estimated SM backgrounds and different choices of neutral gauge boson (Z′) masses generated based on the LV scenario, with dark matter mass ($M_{\chi_1} = 1$ GeV).

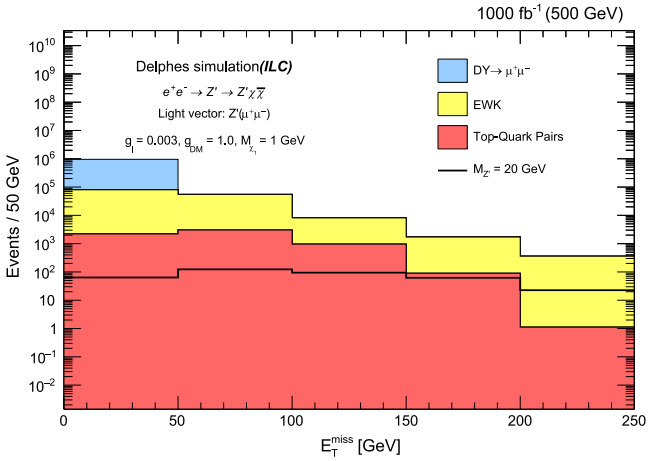

FIG. 5. The distribution of the missing transverse energy, after applying selection(i) summarized in Table IV; for the expected SM backgrounds, and mass of Z' ($M_{Z'} = 20$ GeV) produced by the LV scenario, with mass of dark matter ($M_{\chi_1} = 1$ GeV).

dimuon to a small range around the mass of the neutral gauge boson Z′, thus, it is required that $0.9 \times M_{Z'} < M_{\mu^+\mu^-} < M_{Z'} + 25$ as suggested in [24]. The second is the relative difference between the transverse energy of dimuon ($E_T^{\mu^+\mu^-}$) and the missing transverse energy (E_T^{miss}), it has been selected to be less than 0.4. (i.e. $|E_T^{\mu^+\mu^-} - E_T^{\text{miss}}|/E_T^{\mu^+\mu^-} < 0.4$). The third one is $\Delta\phi_{\mu^+\mu^-,\vec{E}_T^{\text{miss}}}$, which is defined as difference in the azimuth angle between the dimuon direction and the missing transverse energy direction (i.e. $\Delta\phi_{\mu^+\mu^-,\vec{E}_T^{\text{miss}}} = |\phi^{\mu^+\mu^-} - \phi^{\text{miss}}|$), it has been selected to be greater than 2.9 rad. The fourth cut is the angular distance (or angular separation) between two opposite-sign muons [$\Delta R(\mu^+\mu^-)$], it has to be less than 1.8.

The graphs, presented in Fig. 6, illustrate the distributions of certain variables for the signal presentation of the simplified model relating to the light vector scenario. These variables are presented alongside SM backgrounds for dimuon events that pass selection (i). The first variable is denoted as $|E_T^{\mu^+\mu^-} - E_T^{\text{miss}}|/E_T^{\mu^+\mu^-}$, and its graph is shown in the plot 6(a). The second variable is denoted as $\Delta\phi_{\mu^+\mu^-,\vec{E}_T^{\text{miss}}}$, and its graph is shown in the plot 6(b). The third variable is the angular distance[$(\Delta R(\mu^+\mu^-)$], and its graph is presented in the plot 6(c). The model was generated with a neutral gauge boson mass of $M_{Z'} = 20$ GeV, and dark matter mass of $M_{\chi_1} = 1$ GeV. These distributions are scaled to one. The vertical dashed lines in these figures correspond to the chosen cut value for each variable.

V. RESULTS

The shape-based analysis has been used based on the missing transverse energy distributions (E_T^{miss}), which are good discriminate variables since the signals distributions

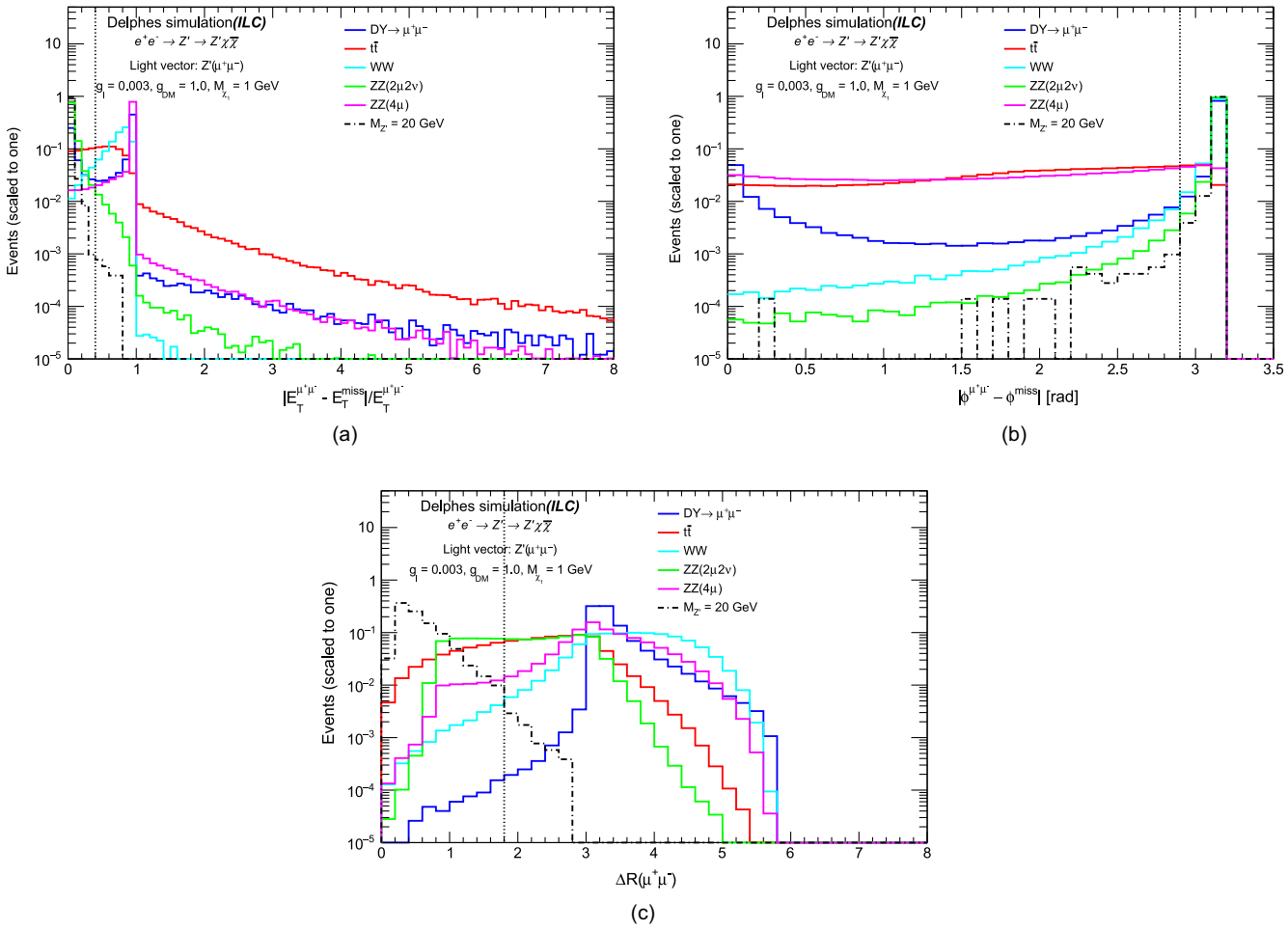

FIG. 6. The distributions of three variables for dimuon events, where each muon passes the low p_T muon ID discussed in selection (i) in Table IV. The three variables are $|E_T^{\mu^+\mu^-} - E_T^{\rm miss}|/E_T^{\mu^+\mu^-}$ 6(a), $\Delta\phi_{\mu^+\mu^-,\vec{E}_T^{\rm miss}}$ 6(b), and $\Delta R(\mu^+\mu^-)$ 6(c). The model corresponds to the LV scenario with $M_{Z'} = 20$ GeV and SM backgrounds. The histograms are normalized to unity to highlight qualitative features, and the vertical dashed lines correspond to the chosen cut value per each variable.

are characterized by relatively large $E_T^{\rm miss}$ values compared to the SM backgrounds. After applying the final event selection listed in Table IV, the missing transverse energy distribution is illustrated in Fig. 7. Table V displays the results of the event selection process for both the SM backgrounds and the signal of the simplified LV scenario. The event selection process includes passing the analysis selection (i) and final selection (i + ii). The signal was generated with masses of a light gauge boson $M_{Z'}$ of 20 GeV, and a dark matter mass M_{χ_1} of 1 GeV,

TABLE IV. Summary of cut-based final event selection used in the analysis.

Step	Variable	Requirements
Selection(i)	p_T^μ (GeV)	> 10
	$\lvert\eta^\mu\rvert$ (rad)	< 2.5
	$\Sigma_i p_T^i / p_T^\mu$	< 0.1
Selection(ii)	Mass window (GeV)	$0.9 \times M_{Z'} < M_{\mu^+\mu^-} < M_{Z'} + 25$
	$\Delta\phi_{\mu^+\mu^-,\vec{E}_T^{\rm miss}}$	> 2.9
	$\lvert E_T^{\mu^+\mu^-} - E_T^{\rm miss}\rvert / E_T^{\mu^+\mu^-}$	< 0.4
	$\Delta R(\mu^+\mu^-)$	< 1.8

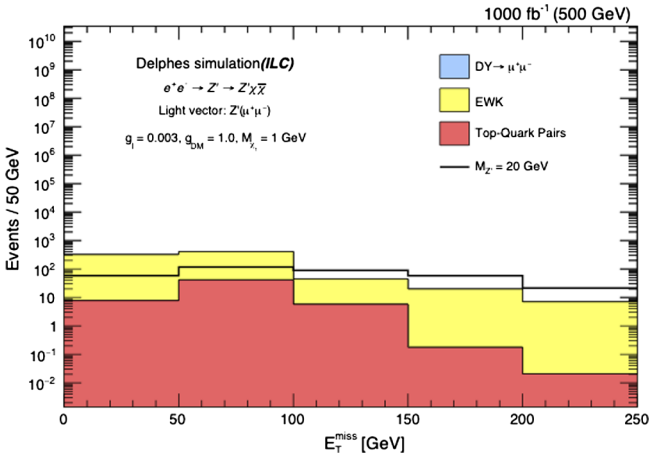

FIG. 7. The distribution of the missing transverse energy, after applying the final analysis selection(i + ii) listed in Table IV, for the expected SM background and one signal benchmark corresponding to the LV with $M_{Z'} = 20$ GeV is superimposed.

corresponding to an integrated luminosity of 1000 fb^{-1}. The uncertainties in the results comprise both statistical and systematic components, which are summed in quadrature.

The significance of the signal over the background was calculated using the Asimov formula described in [56].

$$S = \sqrt{2 \times \left((N_s + N_b) \log\left(1 + \frac{N_s}{N_b}\right) - N_s \right)}, \quad (1)$$

where N_s and N_b are the number of signals and a total of SM background events passing the selections (i + ii) listed in Table IV.

To understand the necessary $M_{Z'}$ values to observe a deviation or a discovery, we have estimated the signal significance (S) by varying values of $M_{Z'}$ for events passing the final selection listed in Table IV. Figure 8 shows the signal significance versus $M_{Z'}$ plotted at different dark matter masses (M_{χ_1}) while using polarized electron-positron beams.

We used the profile likelihood method to analyze our results statistically and performed a statistical test. We used the modified frequentist construction CLs [57,58], which is based on the asymptotic approximation [56], to derive exclusion limits on the product of signal cross sections and the branching fraction Br($Z' \to \mu\mu$) at a 95% confidence level.

In the mono-Z′ model, the 95% upper limit on the cross section times the branching ratio for the LV simplified scenario is shown in Fig. 9. The result is presented for the muonic decay of the Z′ and with coupling constant values of $g_l = 0.003$ and $g_{\rm DM} = 1.0$, for an integrated luminosity of 1000 fb^{-1}. The limits are illustrated for dark matter mass M_{χ_1} values of 1 GeV in 9(a), 150 GeV 9(b), and 170 GeV 9(c), which are represented by the black solid

TABLE V. The table displays the number of events that passed the pre-selection (middle column) and the full selection (right column) criteria, as obtained from simulations for backgrounds and a signal. The simulations were performed with a luminosity of 1000 fb^{-1} at $\sqrt{s} = 500$ GeV. The signal sample corresponds to the simplified-model scenario LV with $M_{Z'} = 20$ GeV, $M_{\chi_1} = 1$ GeV, $g_{\rm DM} = 1.0$ and $g_l = 0.003$. The total uncertainties, including both the statistical and systematic components, have been taken into account for the simulated signal and background samples.

Process	No. of events passing (i)	No. of events passing (i + ii)
DY $\to \mu^+\mu^-$	875756 ± 87581	0 ± 0
$t\bar{t} \to \mu^+\mu^- + 2b + 2\nu$	6293 ± 634	55 ± 9
WW $\to \mu^+\mu^- + 2\nu$	136029 ± 13608	732 ± 78
ZZ $\to \mu^+\mu^- + 2\nu$	2515 ± 257	12 ± 4
ZZ $\to 4\mu$	463 ± 51	0 ± 0
Sum Bkgs	1021055 ± 102111	799 ± 85
Signal of LV scenario (at $M_{Z'} = 20$ GeV and $M_{\chi_1} = 1$ GeV)	366 ± 41	345 ± 39

curves. The vertical dotted red line indicates the upper limit value.

Figure 10 shows the limit on the cross sections times the branching ratios for the muonic decay channel of the Z′ boson as functions of the mediator's mass ($M_{Z'}$) and the mass of the dark matter (M_{χ_1}). The region inside the contour is excluded for the benchmark scenario where $g_l = 0.003$ and $g_{\rm DM} = 1.0$. We used an integrated luminosity of 1000 fb^{-1}. This limit shows that the invariant mass range from 20 to 80 GeV is excluded for $M_{\chi_1} \in [1, 122]$ GeV.

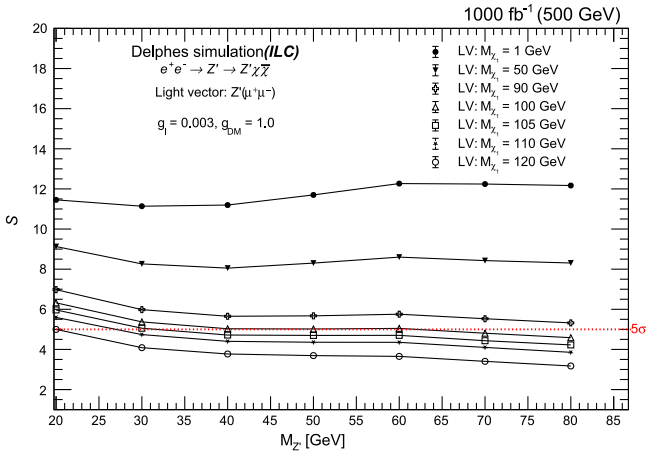

FIG. 8. The significance (S) versus $M_{Z'}$ plotted at different dark matter masses (M_{χ_1}) for events passing the full set of cuts listed in Table IV. The dashed horizontal red line corresponds to $S = 5$.

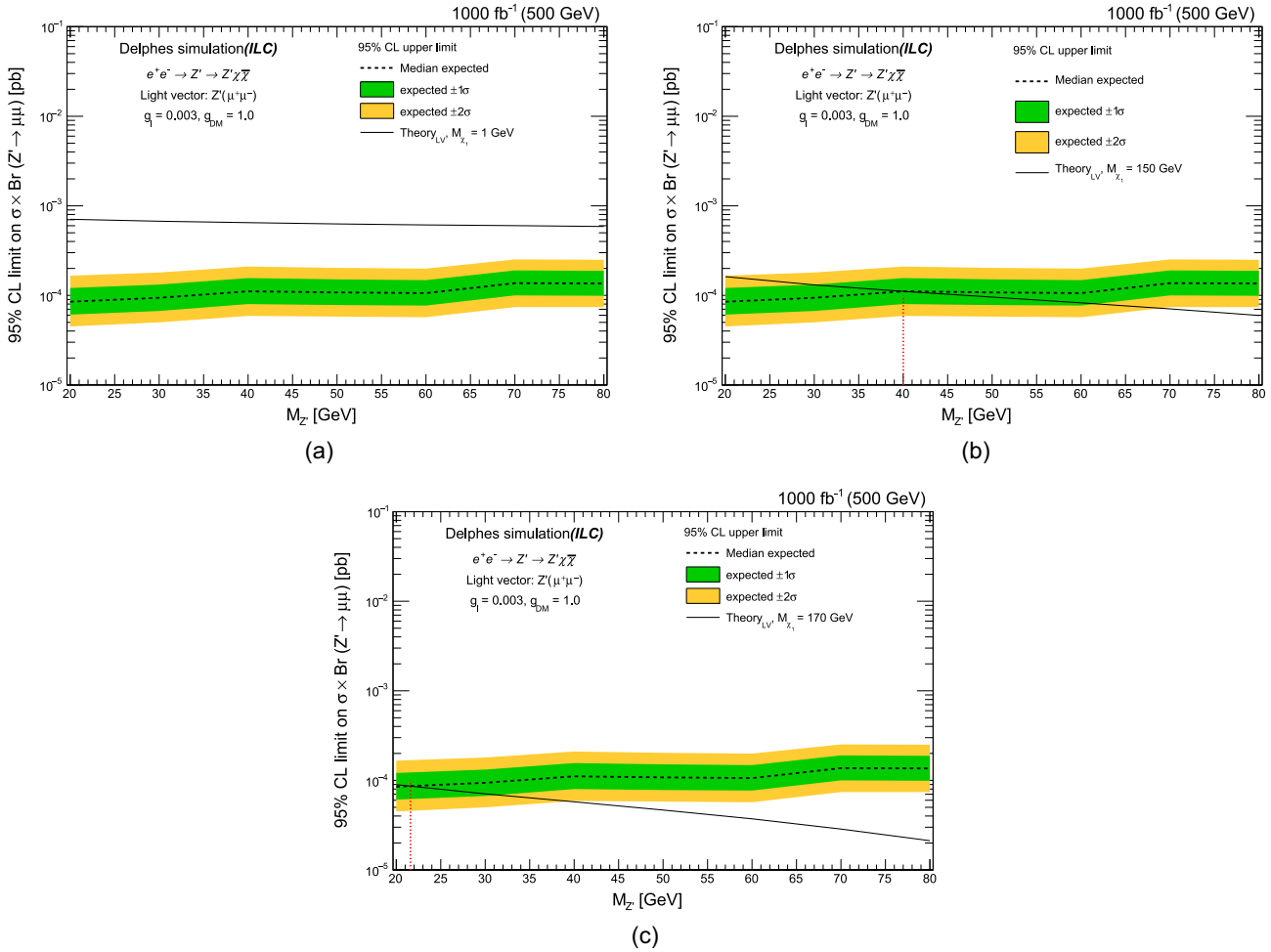

FIG. 9. 95% CL upper limits on the cross section times the branching ratio (expected), as a function of the mediator's mass ($M_{Z'}$) based on mono-Z′ model, with the muonic decay of the Z′. The black line represents the light vector scenario with $M_{\chi_1} = 1$ GeV 9(a), 150 GeV 9(b), and 170 GeV 9(c). The vertical dotted red line indicates the upper limit value.

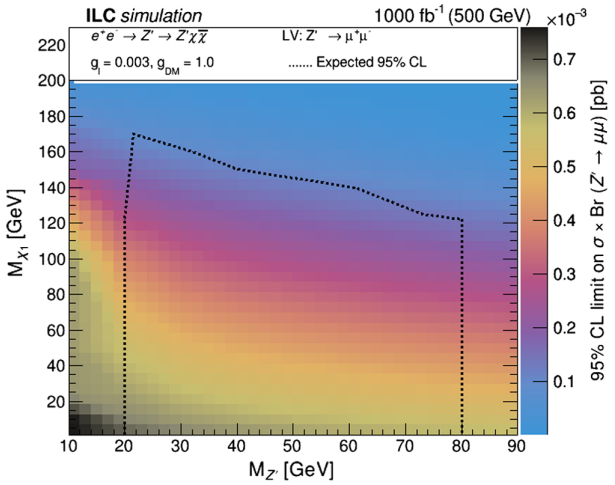

FIG. 10. The 95% CL upper limits on the product of the cross section and branching fraction from the inclusive search, for variations of pairs of the LV scenario parameters ($M_{Z'}$ and M_{χ_1}). The filled region indicates the upper limit. The dotted black curve indicates the expected exclusions for the nominal Z′ cross section.

VI. SUMMARY

The ILC electron-positron collider is an optimal machine for the possible detection of particles from BSM since it delivers a clean signature of unknown particles as dark matter, extra neutral gauge bosons, and Kaluza-Klein excitation concerning the QCD background.

In this view, we have studied the effects of a simplified-model scenario, which is known as light vector (LV), via dark matter pair production associated with a Z′ boson at the ILC. The LV signal samples have been simulated based on electron-positron collisions corresponding to the foreseen ILC RUN I with 500 GeV center of mass energy, for an integrated luminosity of 1000 fb^{-1}. Results from the muonic decay mode of Z′ are discussed, with fixing the values of the coupling constants to be $g_{\mathrm{DM}} = 1.0$, $g_l = 0.003$. Given that the polarized degrees of electron and positron beams are $P_{e^-} = 0.8$, $P_{e^+} = -0.3$ respectively at the ILC.

We observed a significant reduction in the SM backgrounds without affecting the signal strength, using appropriate cuts (listed in Table IV) for the light vector scenario.

If this signal is not observed at the ILC, we set upper limits on the masses of Z′ and dark matter (χ_1) at the 95% CL for the charged muonic channel decay of Z′. Limits have been set for light vector scenario with $g_l = 0.003$ and $g_{\mathrm{DM}} = 1.0$, excluding the invariant mass range from 20 to 80 GeV for $M_{\chi_1} \in [1, 122]$ GeV, nevertheless excluding $M_{\chi_1} = 170$ GeV at $M_{Z'} = 21.5$ GeV.

ACKNOWLEDGMENTS

The author of this paper would like to thank Tongyan Lin, co-author of [24] for providing us with the Universal FeynRules Output (UFO) model files, helping us to generate the signal events, and cross-checking the results.

[1] F. Halzen and A. D. Martin, *Quarks And Leptons: An Introductory Course In Modern Particle Physics* (John Wiley & Sons, New York, 1984), ISBN: 0471887412, 9780471887416.
[2] The ATLAS Collaboration, Observation of a new particle in the search for the Standard Model Higgs boson with the ATLAS detector at the LHC, Phys. Lett. B **716**, 1 (2012).
[3] The CMS Collaboration, Observation of a new boson at a mass of 125 GeV with the CMS experiment at the LHC, Phys. Lett. B **716**, 30 (2012).
[4] Planck Collaboration, Planck 2015 results. XIII. Cosmological parameters, Astron. Astrophys. **594**, A13 (2016).
[5] Planck Collaboration, Planck 2018 results, VI. Cosmological parameters, Astron. Astrophys. **641**, A6 (2020).
[6] C. Lage and G. Farrar, The bullet cluster is not a cosmological anomaly, J. Cosmol. Astropart. Phys. 02 (2015) 038.
[7] P. Langacker, *The Standard Model and Beyond* (CRC Press Taylor & Francis Group, Boca Raton, FL, 2010), ISBN 9781420079067.
[8] M. Cvetic and S. Godfrey, Discovery and identification of extra gauge bosons, arXiv:hep-ph/9504216.
[9] A. Leike, The phenomenology of extra neutral gauge bosons, Phys. Rep. **317**, 143 (1999).
[10] M. Cvetic, P. Langacker, and B. Kayser, Determination of g_R/g_L in left-right symmetric models at hadron colliders, Phys. Rev. Lett. **68**, 2871 (1992).
[11] S. Dimopoulos and H. Georgi, Softly broken supersymmetry and SU(5), Nucl. Phys. **B193**, 150 (1981).
[12] CMS Collaboration, Search for resonant and nonresonant new phenomena in high-mass dilepton final state at $\sqrt{s} = 13$ TeV, J. High Energy Phys. 07 (2021) 208.
[13] ATLAS Collaboration, Search for high-mass dilepton resonances using 139 fb^{-1} of pp collision data collected at $\sqrt{s} = 13$ TeV with the ATLAS detector, Phys. Lett. B **796**, 68 (2019).
[14] Krovi AniruDF, Low Ian, and Zhang Yue, Broadening dark matter searches at the LHC: Mono-X versus darkonium channels, J. High Energy Phys. 10 (2018) 026.
[15] CMS Collaboration, Search for new physics in final states with an energetic jet or a hadronically decaying W or Z boson and transverse momentum imbalance at $\sqrt{s} = 13$ TeV, Phys. Rev. D **97**, 092005 (2018).
[16] ATLAS Collaboration, Search for dark matter in events with a hadronically decaying vector boson and missing transverse momentum in pp collisions at $\sqrt{s} = 13$ TeV with the ATLAS detector, J. High Energy Phys. 10 (2018) 180.
[17] CMS Collaboration, Search for new physics in the monophoton final state in proton-proton collisions at $\sqrt{s} = 13$ TeV, J. High Energy Phys. 10 (2017) 073.
[18] ATLAS Collaboration, Search for dark matter in association with an energetic photon in pp collisions at $\sqrt{s} = 13$ TeV with the ATLAS detector, J. High Energy Phys. 02 (2021) 226.
[19] CMS Collaboration, Search for dark matter particles produced in association with a Higgs boson in proton-proton collisions at $\sqrt{s} = 13$ TeV, J. High Energy Phys. 03 (2020) 025.
[20] ATLAS Collaboration, Search for dark matter produced in association with a standard model Higgs boson decaying into b-quarks using the full Run 2 dataset from the ATLAS detector, J. High Energy Phys. 11 (2021) 209.
[21] ATLAS Collaboration, Search for dark matter in events with missing transverse momentum and a Higgs boson decaying into two photons in pp collisions at $\sqrt{s} = 13$ TeV with the ATLAS detector, J. High Energy Phys. 10 (2021) 013.
[22] ATLAS Collaboration, Search for a new Z′ gauge boson in 4μ events with the ATLAS experiment, J. High Energy Phys. 07 (2023) 090.
[23] CMS Collaboration, Search for an $L_\mu - L_\tau$ gauge boson using $Z \to 4\mu$ events in proton-proton collisions at $\sqrt{s} = 13$ TeV, Phys. Lett. B **792**, 345 (2019).
[24] Marcelo Autran, Kevin Bauer, Tongyan Lin, and Daniel Whiteson, Mono-Z′: Searches for dark matter in events with a resonance and missing transverse energy, Phys. Rev. D **92**, 035007 (2015).
[25] ATLAS Collaboration, Search for a new leptonically decaying neutral vector boson in association with missing transverse energy in proton-proton collisions at $\sqrt{s} =$ 13 TeV with the ATLAS detector, CERN-LHC-ATLAS, Report No. ATLAS-CONF-2023-045, 2023.
[26] LEP Collaborations *et al.*, A combination of preliminary electroweak measurements and constraints on the standard model, arXiv:hep-ex/0312023.
[27] Arnab Dasgupta, P. S. Bhupal Dev, Tao Han, Rojalin Padhan, Si Wang, and Keping Xie, Searching for heavy leptophilic Z': From lepton colliders to gravitational waves, J. High Energy Phys. 12 (2023) 011.
[28] W. Altmannshofer, S. Gori, S. Profumo, and F. S. Queiroz, Explaining dark matter and B decay anomalies with an $L_\mu - L_\tau$ model, J. High Energy Phys. 12 (2016) 106.

[29] LSND Collaboration, Measurement of electron-neutrino-electron elastic scattering, Phys. Rev. D **63**, 112001 (2001).
[30] TEXONO Collaboration, Measurement of $\bar{\nu}_{e^-}$ electron scattering cross-section with a CsI(Tl) scintillating crystal array at the Kuo-Sheng nuclear power reactor, Phys. Rev. D **81**, 072001 (2010).
[31] IceCube Collaborations, All-favor constraints on nonstandard neutrino interactions and generalized matter potential with three years of IceCube DeepCore data, Phys. Rev. D **104**, 072006 (2021).
[32] J. Angle *et al.* (XENON10 Collaboration), Search for light dark matter in XENON10 data, Phys. Rev. Lett. **107**, 051301 (2011); **110**, 249901(E) (2013).
[33] E. Aprile *et al.* (XENON100 Collaboration), Observation and applications of single-electron charge signals in the XENON100 experiment, J. Phys. G **41**, 035201 (2014).
[34] E. Aprile *et al.*, Light dark matter search with ionization signals in XENON1T, Phys. Rev. Lett. **123**, 251801 (2019).
[35] L. Barak *et al.* (SENSEI Collaboration), SENSEI: Direct-detection results on sub-GeV dark matter from a new skipper CCD, Phys. Rev. Lett. **125**, 171802 (2020).
[36] C. Cheng *et al.* (PandaX-II Collaboration), Search for light dark matter–electron scattering in the PandaX-II experiment, Phys. Rev. Lett. **126**, 211803 (2021).
[37] Louis Hamaide and Christopher McCabe, Fueling the search for light dark matter-electron scattering with spherical proportional counters, Phys. Rev. D **107**, 063002 (2023).
[38] M. Ackermann *et al.* (Fermi-LAT Collaboration), Searching for dark matter annihilation from Milky Way dwarf spheroidal galaxies with six years of fermi large area telescope data, Phys. Rev. Lett. **115**, 231301 (2015).
[39] A. Albert *et al.* (DES and Fermi-LAT Collaborations), Searching for dark matter annihilation in recently discovered milky way satellites with fermi-LAT, Astrophys. J. **834**, 110 (2017).
[40] M. Aguilar *et al.* (AMS Collaboration), Electron and positron fluxes in primary cosmic rays measured with the alpha magnetic spectrometer on the international space station, Phys. Rev. Lett. **113**, 121102 (2014).
[41] L. Accardo *et al.* (AMS Collaboration), High statistics measurement of the positron fraction in primary cosmic rays of 0.5–500 GeV with the alpha magnetic spectrometer on the international space station, Phys. Rev. Lett. **113**, 121101 (2014).
[42] P. A. R. Ade *et al.* (Planck Collaboration), Planck 2015 results - XIII. Cosmological parameters, Astron. Astrophys. **594**, A13 (2016).
[43] T. R. Slatyer, N. Padmanabhan, and D. P. Finkbeiner, CMB constraints on WIMP annihilation: Energy absorption during the recombination epoch, Phys. Rev. D **80**, 043526 (2009).
[44] T. R. Slatyer, Indirect dark matter signatures in the cosmic dark ages. I. Generalizing the bound on s-wave dark matter annihilation from Planck results, Phys. Rev. D **93**, 023527 (2016).
[45] J. Smirnov and J. F. Beacom, TeV-scale thermal WIMPs: Unitarity and its consequences, Phys. Rev. D **100**, 043029 (2019).
[46] G. Steigman, B. Dasgupta, and J. F. Beacom, Precise Relic WIMP abundance and its impact on searches for dark matter annihilation, Phys. Rev. D **86**, 023506 (2012).
[47] R. K. Leane, T. R. Slatyer, J. F. Beacom, and K. C. Ng, GeV-scale thermal WIMPs: Not even slightly ruled out, Phys. Rev. D **98**, 023016 (2018).
[48] J. Brau, Y. Okada, and N. Walker, ILC reference design report volume 1 - Executive summary, arXiv:0712.1950.
[49] A. Djouadi *et al.*, International linear collider reference design report volume 2: Physics at the ILC, arXiv:0709.1893.
[50] N. Phinney, N. Toge, and N. Walker, ILC reference design report volume 3 - Accelerator, arXiv:0712.2361.
[51] T. Behnke *et al.*, ILC reference design report volume 4 - Detectors, arXiv:0712.2356.
[52] Wan Neng, Song Mao, Li Gang, Ma Wen-Gan, Zhang Ren-You, and Guo Jian-You, Searching for dark matter via mono-Z boson production at the ILC, Eur. Phys. J. C **74**, 3219 (2014).
[53] Wolfgang Kilian, Thorsten Ohl, and Jurgen Reuter, WHIZARD—simulating multi-particle processes at LHC and ILC, Eur. Phys. J. C **71**, 1742 (2011).
[54] T. Sjostrand, S. Mrenna, and P. Skands, Pythia 6.4 physics and manual, J. High Energy Phys. 05 (2006) 026.
[55] J. de Favereau, C. Delaere, P. Demin, A. Giammanco, V. Lemaître, A. Mertens, and M. Selvaggi, DELPHES 3, A modular framework for fast simulation of a generic collider experiment, J. High Energy Phys. 02 (2014) 057.
[56] G. Cowan, K. Cranmer, E. Gross, and O. Vitells, Asymptotic formulae for likelihood-based tests of new physics, Eur. Phys. J. C **71**, 1554 (2011); **73**, 2501(E) (2013).
[57] A. L. Read, Presentation of search results: The CLs technique, J. Phys. G **28**, 2693 (2002).
[58] T. Junk, Confidence level computation for combining searches with small statistics, Nucl. Instrum. Methods Phys. Res., Sect. A **434**, 435 (1999).